PAPER

NJC
www.rsc.org/njc

Structural effects on the magnetic properties of ferric complexes in molecular materials or a lamellar $CdPS_3$ host matrix††

Sébastien Floquet,[a] M. Carmen Muñoz,[b] Eric Rivière,[a] René Clément,[a] Jean-Paul Audière[a] and Marie-Laure Boillot*[a]

[a] *Laboratoire de Chimie Inorganique (CNRS UMR 8613), ICMMO, Université Paris-Sud, 91405, Orsay, France. E-mail: mboillot@icmo.u-psud.fr*

[b] *Departament de Física Aplicada, Universitat Politécnica de València, Camino de Vera s/n, 46071, València, Spain*

Received* (in Montpellier, France) *17th September 2003, Accepted 2nd December 2003
First published as an Advance Article on the web 3rd March 2004

The electronic properties of cationic ferric complexes were investigated in molecular materials and in a negatively charged lamellar host matrix. Two cations, $[Fe^{III}(R\text{-}Sal_2Trien)]^+$ [where H_2-R-Sal_2Trien is the hexadentate ligand derived from triethylenetetramine and R-substituted salicylaldehydes (R = 3,5-Cl_2 or 5-OMe)], were first assembled with different anions (NO_3^-, ClO_4^-, PF_6^- or BPh_4^-). The obtained compounds exhibit various magnetic behaviours. $S = 5/2$ high-spin species, $S = 1/2$ low-spin species and $S = 5/2 \leftrightarrow S = 1/2$ spin-crossover complexes were identified from variable-temperature SQUID measurements and, in the case of the two cations associated to ClO_4^- and PF_6^-, were confirmed by their X-ray crystal structures at 293 K. When the ferric cations are intercalated within the van der Waals gap of the lamellar $CdPS_3$ host phase, their structural and electronic characteristics appear to be strongly affected. The incomplete spin crossover observed for $[Fe(5\text{-}OMe\text{-}Sal_2Trien)]_{0.26}Cd_{0.87}PS_3 \cdot nH_2O$ and the low-spin behaviour of $[Fe(3,5\text{-}Cl_2\text{-}Sal_2Trien)]_{0.22}Cd_{0.89}PS_3$ can be partly attributed to a different arrangement of the cationic species in the interlamellar space.

Introduction

The elaboration of spin-crossover materials[1–6] by assembling molecular species with structural blocs[7] is of interest for the tuning of the spin-crossover characteristics by environmental effects[8–12] and also for the processing of materials into thin layers for forthcoming investigations of optical processes. This study has been performed with monocationic ferric chelates $[Fe(R\text{-}Sal_2Trien)]^+$ (where H_2-R-Sal_2Trien derives from triethylenetetramine and R-substituted salicylaldehydes) as they belong to a family of spin-crossover complexes[13–18] whose temperature dependent magnetic properties have been extensively investigated in solution (Scheme 1). The spin-crossover process was shown to be controlled by molecular characteristics such as electronic inductive effects due to the R ligand substituent and also to hydrogen bonding interactions. The high-spin (HS) $\leftrightarrow$ low-spin (LS) transitions are also operative in solid samples. Continuous spin transformations were reported both for such complexes in molecular materials and for close cationic analogues encapsulated in polyelectrolytes,[11] or intercalated in montmorillonite[8] or $CdPS_3$ phases.[9] Very recently, we have reported the spin transition of such a cationic ferric complex $[Fe(5\text{-}OMe\text{-}Sal_2Trien)]^+$ intercalated within a $MnPS_3$ layered magnet.[10] This material provides one rare example of a discontinuous transition of a ferric complex exhibiting hysteresis.

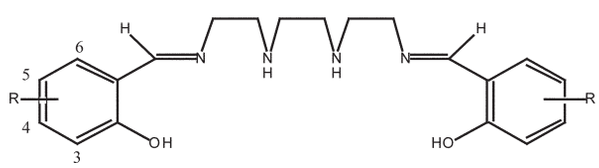

Scheme 1 H_2-R-Sal_2Trien ligand.

The present study is devoted to the characterisation of the structural and magnetic properties of several compounds of this family $[Fe(R\text{-}Sal_2Trien)]Y$ (R = 3,5-Cl_2, 5-OMe; Y = BPh_4^-, PF_6^-, ClO_4^-, NO_3^-) either in the form of a bulk material or of an intercalated material in a diamagnetic $CdPS_3$ host matrix.

Experimental

Materials and measurements

Triethylenetetramine, 3,5-dichlorosalicyladehyde, 5-methoxysalicyladehyde, ferric nitrate and appropriate salts of sodium or ammonium were purchased from Acros or Aldrich and used without further purification.

Infrared spectra were obtained from KBr pellets using a FT-IR Perkin–Elmer spectrum 1000 spectrometer. Magnetic measurements in the 4–400 K temperature range have been carried out on powdered samples (typical weight 15–20 mg) using a Quantum Design SQUID magnetometer (MPMS 5S model). Thermogravimetric analysis (TGA) curves were recorded in air between 293 and 438 K on a Ugine–Eyraud zero balance with a heating rate of 2 K min^{-1}.

Syntheses

Iron(III) complexes. $[Fe(3,5\text{-}Cl_2\text{-}Sal_2Trien)]Y$ [$Y^- = PF_6^-$(**1**), NO_3^- (**2**), ClO_4^- (**3**), BPh_4^- (**4**)] and $[Fe(5\text{-}OMe\text{-}Sal_2Trien)]$

† Electronic supplementary information (ESI) available: Table S1 lists the least-squares planes (*x*, *y*, *z* in crystal coordinates) and deviations from them. Figure S1 shows the powder X-ray diffraction patterns recorded at room temperature for the $CdPS_3$ phase, the pre-intercalate with the NMe^{4+} cation and the intercalated materials **9** and **10**. Figures S2 and S3 display the room temperature IR spectra of **9** and **10**, which are compared to those of **1** and **5**, respectively. Figures S4 and S5 show the EPR spectra of **8** (293 K) and **10** (5 and 291 K). See http://www.rsc.org/suppdata/nj/b3/b311371j/

DOI: 10.1039/b311371j

$Y{\cdot}nH_2O$ [$Y^- = PF_6^-$ and $n = 0.5$ (**5**), NO_3^- (**6**), ClO_4^- (**7**), BPh_4^- (**8**)] were synthesised following standard procedures.[13] Single crystals of compounds **1**, **3**, **5** and **7** were obtained by slow evaporation of methanol–water solutions. Elemental analyses (see Table 1) and FTIR characterisations were consistent with these stoichiometries and formulae.

$CdPS_3$ intercalates 9 and 10. A standard two-step procedure[7a,19] was adopted to intercalate the ferric cationic guest in the $CdPS_3$ host lattice. The tetramethylammonium pre-intercalate $(NMe_4)_{2x}Cd_{1-x}PS_3(H_2O)_y$ was prepared from $CdPS_3$ as previously described[9] and the purity of the pre-intercalate was checked by powder X-ray diffraction [basal spacing of $(NMe_4)_{2x}Cd_{1-x}PS_3(H_2O)_y$ (11.50 Å) and $CdPS_3$ (6.55 Å)]. The intercalation of ferric complexes was carried out by ion-exchanging $(NMe_4)_{2x}Cd_{1-x}PS_3(H_2O)_y$ with [Fe(R-Sal_2Trien)]PF_6. The pre-intercalate (150 mg) was refluxed for 24 or 40 h in an acetonitrile solution (5 mL) of [Fe(3,5-Cl_2-Sal_2Trien)]PF_6 (220 mg) or [Fe(5-OMe-Sal_2Trien)]$PF_6{\cdot}0.5H_2O$ (200 mg) to give **9** or **10**, respectively. Resulting dark brown or dark purple materials were filtered, washed with acetonitrile until the filtrate became colourless and dried in vacuum.

Both microcrystalline samples appear to be well-crystallised as the powder X-ray diffractograms exhibit rather sharp (00*l*) reflections (see spectrum of **9** in Figure S1 in the Electronic supplementary information). Complete disappearance of the (00*l*) reflection of the pre-intercalate (11.50 Å) ascertains the full intercalation of the host lattice. For these lamellar materials, the measured values of the basal spacing (14.60 Å for **9** and 19.30 Å for **10**) span over the range already reported.[9,10]

Elemental analyses of the intercalate materials were consistent with the formulations [Fe(3,5-Cl_2-Sal_2Trien)]$_{0.22}Cd_{0.89}PS_3{\cdot}nH_2O$ (**9**) and [Fe(5-OMe-Sal_2Trien)]$_{0.26}Cd_{0.87}PS_3{\cdot}nH_2O$ (**10**). Anal. calcd (%) for [Fe(3,5-Cl_2-Sal_2Trien)]$_{0.22}Cd_{0.89}PS_3{\cdot}nH_2O$ ($n = 0$; **9**; 347.34 g mol^{-1}): C 15.21, H 1.28, N 3.55, Fe 3.54, Cd 28.80; found: C 15.08, H 1.28, N 3.56, Fe 3.32, Cd 27.79. Anal. (%) calcd for [Fe(5-OMe-Sal_2Trien)]$_{0.26}Cd_{0.87}PS_3{\cdot}nH_2O$ ($n = 0.26$; **10**; 351.42 g mol^{-1}): C 19.55, H 2.24, N 4.15, Fe 4.13, Cd 27.83; found: C 19.99, H 2.23, N 4.33, Fe 3.89, Cd 26.63. From these data, the intercalation ratio $2x$ estimated at 0.22 (0.26) mole of ferric complexes accounts well for the electric charge balance with $1 - x = 0.89$ (0.87) mole of $CdPS_3$ unit for **9** (**10**). The lower stoichiometry of $\mathbf{9} - 2x = 0.22-$ is due to the larger size of the molecular cross section in the layer plane (*vide infra*) as intercalation in the MPS_3 family proceeds until close packing of the guest species is achieved. The elemental analysis and IR data suggest the presence of co-intercalated water in **10** as previously characterised for [Fe(5-OMe-Sal_2-Trien)]$_{0.28}Mn_{0.86}PS_3{\cdot}0.30\ H_2O$.[10] In contrast to this material, TGA measurements performed for **9** do not allow us to detect any weight change upon heating the sample up to 400 K. The solvent molecules possibly co-inserted with cations might be trapped within this lattice because of specific structural constraints.

From the FTIR spectra of **9** and **10** (see Figures S2 and S3 in the ESI), the assignment of numerous vibration bands of ferric cations provides evidence of the unaltered co-ordination cores of these complexes. Due to the ionic exchange, the strong bands of the PF_6^- salt at 835(vs) and 558(s) cm^{-1} were replaced by the intense $\nu(PS_3)$ stretching modes of $CdPS_3$, which were split into three components (551, 583 and 599 cm^{-1}) for **9** and two major and one minor components (552, 599 cm^{-1} and 586 cm^{-1}) for **10**. These features, which depart from the previous observations on [Fe(5-OMe-Sal_2Trien)]$_{0.28}$-$Mn_{0.86}PS_3{\cdot}0.30H_2O$ (556 and 608 cm^{-1}) and pure $CdPS_3$ (563 cm^{-1}), are indicative of a vacancy ratio x lower than 1/6 and hence a less ordered material than the $MnPS_3$ intercalate.[10]

Table 1 Elemental analyses for compounds **1**–**8**

Compound	% C (calcd)	% H (calcd)	% N (calcd)
1 [Fe(3,5-Cl_2-Sal_2Trien)]PF_6	34.66 (34.76)	2.74 (2.92)	8.26 (8.11)
2 [Fe(3,5-Cl_2-Sal_2Trien)]NO_3	39.27 (39.51)	3.22 (3.32)	11.20 (11.52)
3 [Fe(3,5-Cl_2-Sal_2Trien)]ClO_4	37.06 (37.21)	3.25 (3.12)	8.36 (8.68)
4 [Fe(3,5-Cl_2-Sal_2Trien)]BPh_4	60.71 (61.07)	4.63 (4.66)	6.44 (6.48)
5 [Fe(5-OMe-Sal_2Trien)]$PF_6{\cdot}0.5H_2O$	42.22 (42.46)	4.52 (4.70)	8.83 (9.00)
6 [Fe(5-OMe-Sal_2Trien)]NO_3	49.21 (49.82)	5.48 (5.32)	13.23 (13.21)
7 [Fe(5-OMe-Sal_2Trien)]ClO_4	46.47 (46.54)	4.84 (4.97)	9.63 (9.87)
8 [Fe(5-OMe-Sal_2Trien)]BPh_4	69.56 (70.15)	6.17 (6.14)	7.13 (7.11)

X-Ray structural analyses

Structures of compounds **1**, **3**, **5** and **7** were obtained at room temperature. Data collections were carried out on an Enraf–Nonius CAD4 diffractometer with monochromated MoKα radiation ($\lambda = 0.71073$ Å). Lattice parameters were obtained from least-squares refinement of the settings angles of 25 reflections in the range $12° < \theta < 20°$. Lorentz-polarisation corrections were applied and absorption corrections were made. SHELXS97 and SHELXL97[20] were used to solve **1**, **3**, **5** and **7** by direct methods and to refine them by full least-squares refinement. Atomic scattering factors were taken from ref. 20. The final full-matrix least-squares refinement, minimising the function $\Sigma[w(F_0^2 - F_c^2)^2]$ converged to R and wR values (Table 2) larger than 7%. The accuracy of the structures of **1**, **3** and **7** is limited by the quality of the crystals and also by disorder (*vide infra*). Hydrogen atoms were placed in calculated positions and isotropically refined. In Table S1 are reported the least-squares planes (x, y, z in crystal coordinates) and deviations from them.‡

Results and discussion

X-Ray structures

The single crystal X-ray structures of compounds **1**, **3**, **5** and **7** have been determined at 293 K where the iron(III) ions are at least partly in the HS or the LS state [HS fraction estimated from $\chi_M T^{HS} = 4.38$ and $\chi_M T^{LS} = 0.375$ cm^3 mol^{-1} K: $\gamma_{HS} \approx 0.86$ (**1**), ≈0.52 (**3**), ≈0.98 (**5**) and ≈0.09 (**7**)]. Crystal, data collection and refinement parameters for all complexes are given in Table 2. Table 3 contains selected bond lengths and angles. Both [Fe(3,5-Cl_2-Sal_2Trien)]Y complexes with $Y = PF_6^-$ (**1**) and ClO_4^- (**3**) are isostructural and crystallise as *Pccn* ($Z = 4$) with similar unit cell volumes. The PF_6^- (**5**) and ClO_4^- (**7**) salts of [Fe(5-OMe-Sal_2Trien)]$^+$ crystallise in the $P2_1/c$ ($Z = 4$) and $C2/c$ ($Z = 4$) space groups, respectively. The asymmetric units of **1**, **3**, **5** and **7** contain two Fe^{III} cations. The iron(III) cations are localised on the glide planes of *Pccn* (**1** and **3**), the twofold axes of $C2/c$ (**7**) or are in general positions (**5**).

Molecular structures. The molecular structures of these complexes consist of pseudo-octahedrally coordinated metal ions

† CCDC reference numbers 226787–90. See http://www.rsc.org/suppdata/nj/b3/b311371j/ for crystallographic data in .cif or other electronic format.

Table 2 Crystal, data collection and refinement parameters determined for **1**, **3**, **5** and **7** at 293 K. Wavelength (MoK_α) = 0.71073 Å; T = 293(2) K. Wavelength (Mo Kα) = 0.7103 Å.

	1	**3**	**5**	**7**
Empirical formula	$C_{20}H_{20}Cl_4F_6FeN_4O_2P$	$C_{20}H_{20}Cl_5FeN_4O_6$	$C_{22}H_{29}F_6FeN_4O_{4.5}P$	$C_{22}H_{28}ClFeN_4O_8$
Formula weight	691.02	645.50	622.31	567.78
Crystal system	Orthorhombic	Orthorhombic	Monoclinic	Monoclinic
Space group	*Pccn*	*Pccn*	*P*21/*c*	*C*2/*c*
a/Å	10.7371(17)	10.414(2)	11.837(4)	13.0840(15)
b/Å	14.083(3)	13.959(3)	17.134(5)	18.5298(19)
c/Å	17.183(3)	16.933(5)	13.764(5)	10.1690(13)
α/°	90	90	90	90
β/°	90	90	113.08(2)	97.24(1)
γ/°	90	90	90	90
U/Å^3	2598.1(8)	2461.6(10)	2568.0(14)	2445.78(49)
Z	4	4	4	4
μ/mm^{-1}	1.125	1.202	0.733	0.781
Reflect. collect.	1687	2857	3514	1661
Indep. reflect.	1687	2148	3330	1584
R_{int}	—	0.0182	0.065	0.030
R (wR)[a]	0.082 (0.157)	0.0458 (0.1130)	0.095 (0.220)	0.071 (0.204)
R_{all} (wR_{all})	0.251 (0.234)	0.0737 (0.1248)	0.216 (0.295)	0.101 (0.236)

[a] R and wR are given for [$I = 2\sigma(I)$].

with hexadentate ligands. ORTEP drawings of these molecular structures are depicted in Fig. 1 (**1**), Fig. 2 (**7**) and Fig. 3 (**5**). The iron(III) ions are surrounded by two oxygen atoms (O1A, O1B) in cis positions, two imino (N1A, N1B) and two amino (N2A, N2B) nitrogen atoms. This arrangement is consistent with those already reported for salts of [Fe(Sal$_2$-Trien)]$^+$.[16–18] A more detailed comparison of the coordination cores can be achieved from the metal-ligand bond lengths and angles collected in Table 3. We first note the nonequivalency of the sets of two Fe–O1,2, Fe–N1,4 and Fe–N2,3 bonds for complex **5** in contrast to complexes **1**, **3**, **7**. The deviation from octahedral symmetry of the FeN_4O_2 unit is variable along this series, as shown by the set of uneven bond lengths and strained angles. The average Fe–O bond distances [1.876 (**3**), 1.882 (**7**), 1.894 (**1**) and 1.902 (**5**) Å] are by far the shortest as a consequence of the negative charge borne by the phenolic oxygen atom. The Fe–N_{amino} bonds to the amino nitrogen atoms are the largest with average values ranging between 2.022 (**7**), 2.105 (**3**), 2.183 (**1**) and 2.209 (**5**) Å. Effects of π-backbonding between the imino nitrogen atoms and the iron(III) atom are responsible for the intermediate average values found for the Fe–N_{imino} bonds [1.953 (**7**), 2.029 (**3**), 2.090 (**1**) and 2.113 (**5**) Å]. These data lead to an average metal-ligand bond length ⟨Fe–L⟩ increasing as 1.952 (**7**), 2.003 (**3**), 2.056 (**1**) and 2.075 (**5**) Å. With regard to the literature data on ferric Schiff base complexes, these data unambiguously reflect the variations due to the spin state change of the metal ion. Indeed, for [Fe(R-Sal$_2$Trien)]Y,[16–18,21–23] Fe–O bonds are expected to slightly vary from $\langle Fe–O\rangle_{HS}$ = 1.908–1.939 Å to $\langle Fe–O\rangle_{LS}$ = 1.879–1.895 Å. Fe–N_{amino} bonds are the most compressible, varying from $\langle Fe–N_{amino}\rangle_{HS}$ = 2.173–2.215 Å to $\langle Fe–N_{amino}\rangle_{LS}$ = 1.999–2.046 Å; significant modifications are also observed for Fe–N_{imino} bonds with $\langle Fe–N_{imino}\rangle_{HS}$ = 2.081–2.125 Å and $\langle Fe–N_{imino}\rangle_{LS}$ = 1.930–1.944 Å. The corresponding values of the average metal-ligand bond length are equal to $\langle Fe–L\rangle_{HS}$ = 2.058–2.074 Å and

Table 3 Selected ligand-metal bond lengths (Å) and angles (deg) in **1**, **3**, **5** and **7**. For **5**, O(1A), O(1B), N(1A), N(1B), N(2A) and N(2B) should be replaced by O(1), O(2), N(1), N(2), N(3) and N(4)

	1	**3**	**5**	**7**
Fe–O(1A)	1.894(10)	1.876(3)	1.892(9)	1.882(5)
Fe–O(1B)			1.912(8)	
Fe–N(1A)	2.090(13)	2.029(4)	2.113(11)	1.953(7)
Fe–N(1B)			2.096(11)	
Fe–N(2A)	2.183(13)	2.105(4)	2.212(10)	2.022(8)
Fe–N(2B)			2.206(11)	
O(1A)–Fe–O(1B)	105.1(6)	101.7(2)	104.0(4)	96.4(4)
O(1A)–Fe–N(1A)	85.5(6)	89.08(14)	87.7(4)	87.8(3)
O(1B)–Fe–N(1B)			86.2(4)	
O(1A)–Fe–N(1B)	91.3(6)	89.0(2)	96.0(4)	93.0(2)
O(1B)–Fe–N(1A)			101.8(4)	
O(1B)–Fe–N(2A)	89.5(5)	89.9(2)	89.1(4)	89.9(3)
O(1A)–Fe–N(2B)			91.5(4)	
N(1A)–Fe–N(2A)	105.1(5)	80.3(2)	77.2(4)	96.1(3)
N(2B)–Fe–N(1B)			78.4(4)	
N(1A)–Fe–N(2B)	78.9(5)	102.1(2)	92.5(4)	83.0(3)
N(2A)–Fe–N(1B)			97.5(4)	
N(2A)–Fe–N(2B)	81.0(8)	80.9(3)	79.4(4)	84.2(5)

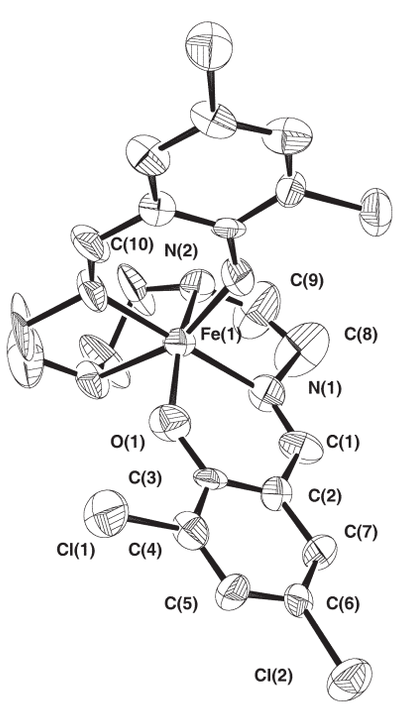

Fig. 1 ORTEP drawing of the Fe^{III} cation in [Fe(3,5-Cl_2-Sal$_2$-Trien)]PF_6 (**1**).

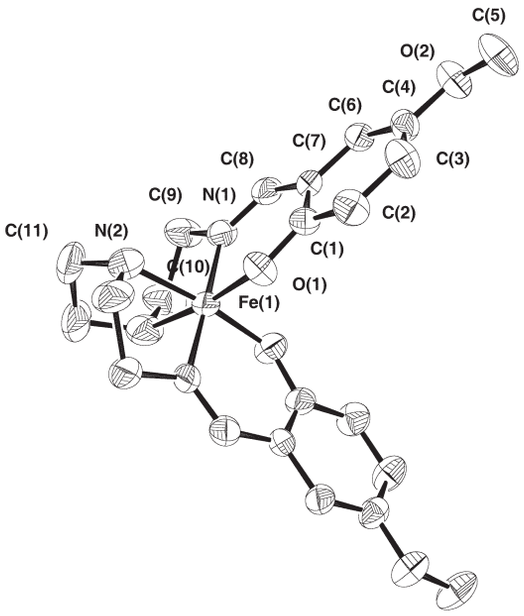

Fig. 2 ORTEP drawing of the Fe^{III} cation in [Fe(5-OMe-Sal_2Trien)]-ClO_4 (**7**).

$\langle Fe–L \rangle_{LS} = 1.937–1.959$ Å. It is inferred from this comparison that **1** and **5** are HS species whereas **7** is a LS species. The sequence of increasing content in HS isomer, $\mathbf{7} < \mathbf{3} < \mathbf{1} < \mathbf{5}$, is consistent with the one deduced from the magnetic measurements at 293 K (*vide infra*).

The coordination of the hexadentate ligand to iron(III) gives rise to three five-membered and two six-membered chelate rings fused together and hence large geometrical constraints, as shown by several bond angles smaller or larger than 90° (see Table 3). These steric strains, which are mainly due to the five-membered chelate rings, give rise to larger distortions from the octahedral geometry when the metal-ligand bond length is itself larger, therefore increasing with HS content. For the sake of comparison of the octahedral distortion, the Σ parameter,[24] corresponding to the sum of the absolute values of the deviation from 90° of the twelve bond angles, Φ_i, $\Sigma = \sum_{i=1}^{12} (\Phi_i - 90)$ was calculated. The Σ values can be classified as 49.0 (**7**), 68.4 (**3**), 85.3 (**5**) and 89.1° (**1**). Again, consistency is found between structural and magnetic data since this order roughly corresponds to increasing values of the HS fraction. From the literature data restricted to [Fe(R-Sal_2Trien)]Y complexes[16–18,21–23] and the present ones, it is found that the Σ values span over a range of 43.4°[16]–49.0° to 85.3°–95.2°[17] for fully LS and HS species, respectively. The planes defined by the three groups of four equatorial ligand donor atoms (see Table S1, ESI) are found to deviate more or less from true planarity but they are nearly orthogonal to each other. The shift of the iron atom from the centre of the octahedron appears to be larger for the species with a higher HS content ([0.0681 (**7**), 0.0034–0.0027 (**3**), 0.2529 (**1**), 0.1697 (**5**) Å]. It is evident in Figs. 1, 2 and 3 that the 293 K molecular structures of **1**, **5** and **7** present rather large thermal parameters. Large and anisotropic ellipsoids are mainly observed for the disordered water atoms of **5** (O), the hexafluorophosphate atoms of **1** (F), **5** (F), the perchlorate atoms of **3** (O) and **7** (O), for the ethylenic carbon atoms of the chelating ligand of **1**, **3** and **7** and finally for the Cl and CH_3O phenyl substituents of **3** and **5**. These features that show some dynamic disorder might contribute to a slight increase of the intermolecular distances.

Molecular packing. *[Fe(3,5—Cl_2-Sal_2Trien)]Y complexes.* In Fig. 4, the molecular packing of **1**, similar to the one of **3**, is shown in the *ac* plane. The crystal lattice of these compounds consists of a double layer of cationic molecules arranged in a zigzag manner (*ab* plane) and associated to PF_6^- or ClO_4^- anions located slightly above or under these layers of cations. In the perpendicular direction (*c*), the packing consists of cations closely packed along their pseudo-molecular symmetry axis. The intermetallic distances that are the shortest in this direction are equal to 8.467 (**3**) and 8.591 (**1**) Å. In the case of **3**, [Fe(3,5-Cl_2-Sal_2Trien)]$^+$ complexes are hydrogen bonded *via* the two amino groups of the ligand to oxygen atoms of the ClO_4^- anions. These weak hydrogen bonding interactions characterised by O3–N2A distances of 3.181 Å and an O3–H2–N2A angle of 158.35° contribute to stabilise **3** in an anhydrous form. These intermolecular

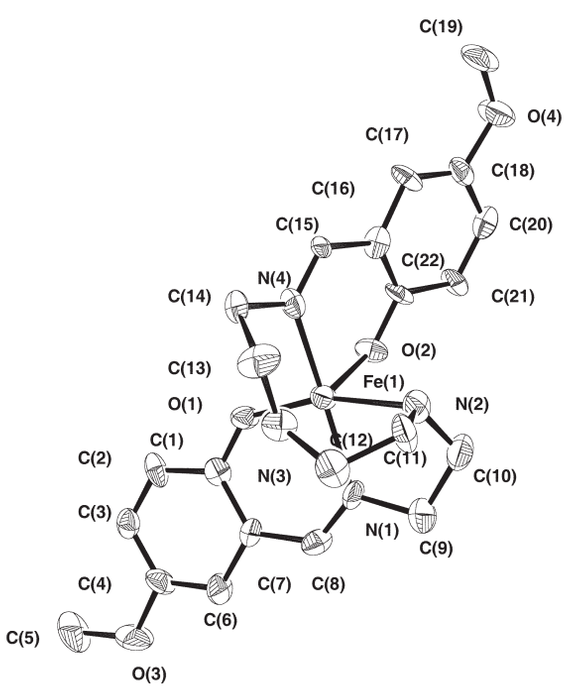

Fig. 3 ORTEP drawing of the Fe^{III} cation in [Fe(5-OMe-Sal_2-Trien)]$PF_6 \cdot 0.5H_2O$ (**5**).

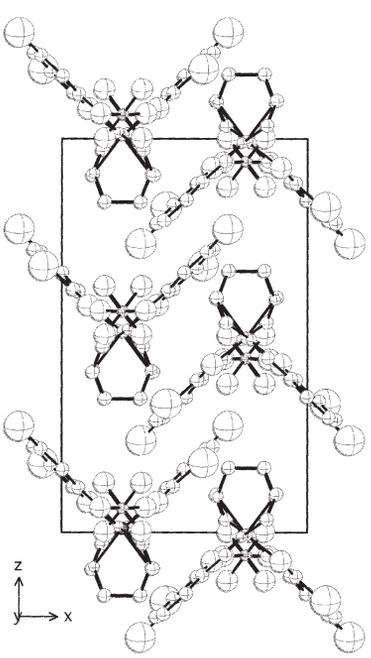

Fig. 4 Packing diagram for **1** in the *ac* plane. Hydrogen atoms are omitted for clarity.

interactions lead to an unique type of NH group and a high symmetry for the complexes. They were also reported for ferric [Fe(Sal_2Trien)]Cl·2H_2O, [Fe(Sal_2Trien)]NO_3·H_2O and [Fe(Sal_2Trien)]PF_6.[16,17]

[Fe(5-OMe-Sal_2Trien)]Y complexes. In Fig. 5, the molecular packing of **7** shown in the *bc* plane again consists of a double layer (*ac* plane) with a zigzag arrangement of cations. Rather large intermetallic distances are observed between the cationic species localised in this plane. In the perpendicular direction (*b*), the cations are aligned along their pseudo-molecular axis but in contrast to **1** and **3** they are alternatively separated by ClO_4^- anions. Such a position of the anions leads to larger intermetallic distances of 11.342 Å along this direction. The ClO_4^- anions are slightly hydrogen-bonded to the amine nitrogen atom N of the two cationic species (*d*O3–N2A = 3.116 Å, angle N2A–H2–O3 150.45°) and form a juxtaposition of alternating complexes and anions.

The structure of the hydrated compound **5** differs from the previous ones. In this case, all the metal-ligand bonds are inequivalent. Both the Fe–L distances and bond angles are typical of an iron(III) ion in the HS state as confirmed by SQUID measurements. Fig. 6 shows the packing diagram of [Fe(5-OMe-Sal_2Trien)]PF_6·0.5H_2O in the *bc* plane. The crystallisation of this compound with water molecules favours the formation of cationic layers (*ab* plane) consisting of a new zigzag arrangement of pairs of cations, each pair alternating with a water molecule. Because of the presence of this disordered water molecule, which is hydrogen-bonded to the amino group N2–H2 of one cation of the neighbouring ribbons (*d*O5–N2 = 2.978 Å), the closest intermetallic distance between iron atoms belonging to different pairs is 9.37 Å. Two types of cations having their pseudo-molecular axes close to the *c* direction are found to be alternatively packed with very close intermetallic distances of 6.916 Å.

Magnetic properties

In Fig. 7 is shown the temperature dependence of the $\chi_M T$ product (where χ_M is the molar magnetic susceptibility) for compounds **5**–**8** and **10**, together with those of **1**–**4** and **9**, which have been previously reported between 10–300 K.[11] As earlier mentioned, these data reveal magnetic behaviours of the cationic complexes in the solid state that vary with the nature of the counter ion or matrix for molecular or intercalated materials, respectively.

Molecular materials. Let us briefly recall that **1** and **3** undergo a gradual spin-crossover process, whereas **2** and **4** are HS and LS species, respectively. [Fe(5-OMe-Sal_2Trien)]PF_6·0.5H_2O (**5**) and [Fe(5-OMe-Sal_2Trien)]NO_3 (**6**) remain in the HS state [$\chi_M T$ = 4.31 (**5**) and 3.91 (**6**) cm^3 mol^{-1} K at 293 K]. [Fe(5-OMe-Sal_2Trien)]ClO_4 (**7**) is trapped in the LS state up to 250 K with the very beginning of a LS ↔ HS conversion taking place on heating ($\chi_M T$ = 0.73 cm^3 mol^{-1} K at 293 K). Finally, intermediate $\chi_M T$ values recorded for the BPh_4^- salt **8** are ascribed to a mixture of HS and LS species (at 20 K, $\chi_M T$ = 2.56 cm^3 mol^{-1} K, $\gamma_{HS} \sim 0.54$), as confirmed by the 77 K EPR spectrum (see Figure S4, ESI). A slight increase of this value is observed upon heating the sample up to 300 K ($\chi_M T$ = 3.14 cm^3 mol^{-1} K).

This set of data contrasts to those reported for these [Fe(R-Sal_2Trien)]Y complexes in solution. Indeed, it was shown by magnetic susceptibility measurements in solution that electron-donating and electron-withdrawing R ligand substituents stabilise HS and LS states, respectively.[13] We note that this effect might be responsible for the net increase of the ligand field strength characterised here for the PF_6^- salts, **5** (R = 5-OMe) < **1** (R = 3,5-Cl_2), but this observation appears to be unique in the investigated series (see, for example, the data for ClO_4^- salts). Therefore, it clearly appears that the magnetic

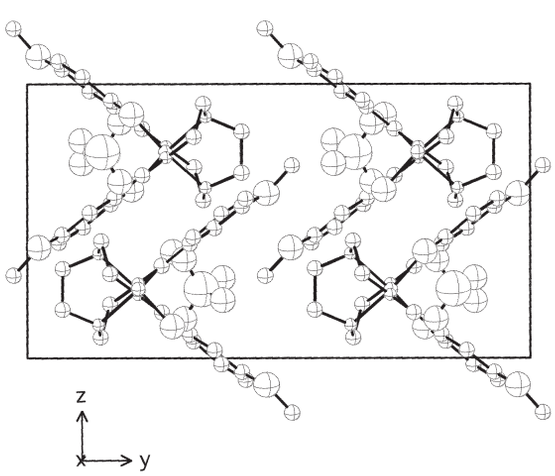

Fig. 5 Packing diagram for **7** in the *bc* plane. Hydrogen atoms are omitted for clarity.

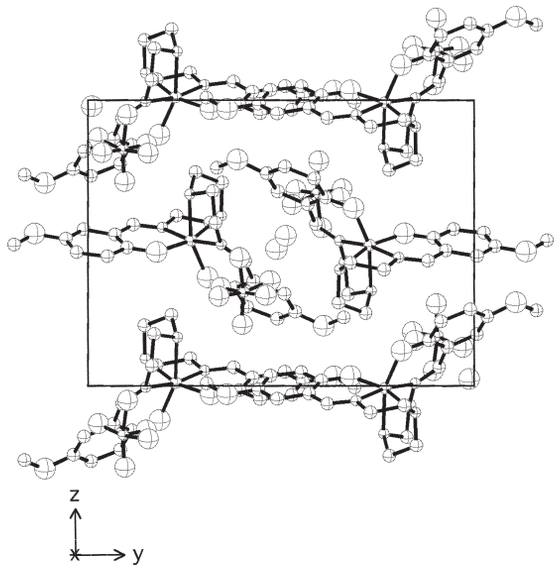

Fig. 6 Packing diagram for **5** in the *bc* plane. Hydrogen atoms are omitted for clarity.

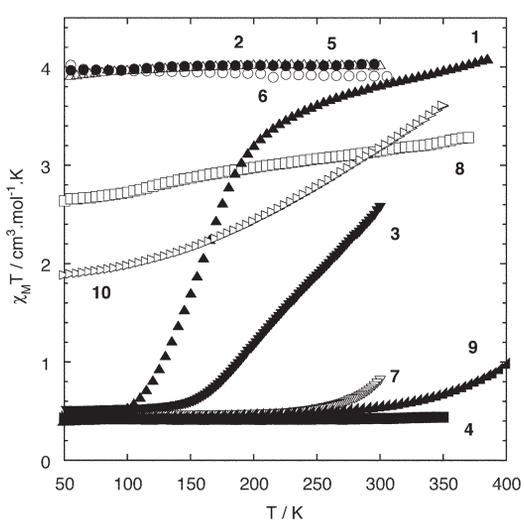

Fig. 7 Temperature dependence of the $\chi_M T$ product (χ_M being the molar magnetic susceptibility) of [Fe(5-OMe-Sal_2Trien)]Y [(△) **5**, (○) **6**, (▽) **7**, (□) **8**] and [Fe(3,5-Cl_2-Sal_2Trien)]Y [(▲) **1**, (●) **2**, (▼) **3**, (■) **4**] complexes. For the intercalated $CdPS_3$ materials [(◂) **9**, (▷) **10**], the $\chi_{Fe} T$ value refers to one mole of ferric cation. The data related to [Fe(3,5-Cl_2-Sal_2Trien)]Y (**1**–**4** and **9**) were partly described in ref. 11.

behaviours of these solid compounds result from major effects due to the arrangement and packing of the complexes in the lattice. In the case of the two isostructural [Fe(3,5-Cl_2-Sal_2-Trien)]Y (**1** and **3**) compounds, the comparison of the transition curves showing a relative HS stabilisation for the salt of the anion of larger size is consistent with an additional effect of chemical pressure due to the crystal lattice constraints.[1,25] The very limited spin-crossover process characterised for **8** can be due to a mixture of different solids or more likely to the presence of structurally different cationic molecules in the unit cell, as reported, for example, in ref. 17. The amorphous character of this powdered compound has prevented any structural investigation of this assumption.

Weak hydrogen-bonding interactions have been characterised between the ligand backbone (the two N2H2 groups) of the cations and ClO_4^- anions in **3** and **7**. They give rise to infinite chains of interacting cations and anions. It was recognised from studies of these compounds in solutions that this feature may contribute to the relative stabilisation of the LS state of **3** and **7**. This contrasts with the data related to the hydrated compound **5**. For this HS compound, hydrogen bonds are found between a water molecule occupying one of two possible sites and an unique ferric complex cation. We can suggest that in this case the inductive effect provided by this discrete interaction between the N2H2 group and water molecule is not strong enough and/or these disordered solvent molecules lead to some intermolecular spacing and structural relaxation responsible for the relative stabilisation of the HS state and an original packing of strongly distorted molecules.

Finally, the spin-crossover processes in this series of molecular compounds are found to be gradual in spite of the arrangement of anions and cations interconnected through hydrogen bonds. This feature is fully consistent with the previously reported studies and shows that this type of crystalline structure, common to **1**, **3** and also to **7**, accommodates quite easily the change of the molecular volume due to the spin-crossover.

Intercalated complexes in the layered material $CdPS_3$. The temperature dependence of the $\chi_{Fe}T$ product of **9** and **10** (χ_{Fe} being related to one mole of Fe) is shown in Fig. 7. For **9**, the ferric ions are trapped in the LS state in a large range of temperature as confirmed by EPR measurements.[11,19] However, the data collected at high temperature suggest that they undergo a very limited spin crossover ($\chi_{Fe}T = 1.0$ cm^3 mol^{-1} K at 400 K). For compound **10**, the occurrence of a gradual and incomplete transition is shown by the $\chi_{Fe}T$ *vs.* T curve ($\chi_{Fe}T = 1.8$ and 3.1 cm^3 mol^{-1} K at 10 and 290 K, respectively). The spin crossover and the presence of residual HS species suggested by the $\chi_{Fe}T$ value at 10 K ($\gamma_{HS} \approx 0.33$) are confirmed by EPR measurements (see Figure S5, ESI) performed between 4 and 291 K. These data recorded at increasing and decreasing temperatures are strictly superimposable for temperature values lower than 300 K. The characteristics of this spin-crossover curve (the smoothness and temperature at which the transition is half complete, $T_{1/2} \sim 290$ K) roughly compare to those of the corresponding $MnPS_3$ intercalate extrapolated from the magnetic data. Finally, heating of the sample to 350 K causes an irreversible increase of the HS content ($\Delta\gamma_{HS} \approx 4\%$) and a new gradual curve of $\chi_{Fe}T$ *vs.* T ($\chi_{Fe}T = 3.7$ cm^3 mol^{-1} K at 350 K). This observation again parallels the one obtained for [Fe(5-OMe-Sal_2Trien)]$^+$ intercalated in the $MnPS_3$ phase,[10] which is due to the removal of a fraction of water molecules co-intercalated with the cations.

The rather high content of species trapped in the HS state is likely to result from the presence of inhomogeneities or structural defects.[26,27] We note that cations in the $CdPS_3$ intercalate should be less densely packed than in the $MnPS_3$ one as the intercalation ratio ($x = 0.13$) and the interlayer spacing ($d = 19.30$ Å) in $CdPS_3$ are slightly lower and larger, respectively, than the corresponding values in $MnPS_3$ ($x = 0.14$ and $d = 19.10$ Å).[10]

To go further with the comparison of the magnetic behaviours of **9** and **10**, discussion can be focused both on the structural parameters of these intercalated MPS_3 materials and those of the molecular [Fe(R-Sal_2Trien)]Y samples. A specific feature of the $[guest]_{2x}Cd_{1-x}PS_3$ intercalation compounds is that the uptake of guest species proceeds until the latter become closed packed. Moreover, the structure of the intercalate derives from the tight stacking of negatively charged $M_{1-x}PS_3$ layers and positively charged iron complexes. Therefore, it should be emphasised that the iron complexes are not more diluted in the intercalated state than they are in any compound where a molecular cation coexists with an anion. Comparison of the values of the two basal spacings (14.6 Å for **9** and 19.3 Å for **10**) with the thickness of the MPS_3 slabs (6.55 Å for M^{II} = Cd) leads to the conclusion that the inserted iron complexes occupy 55% (**9**) and 65% (**10**) of the crystal space. These values compare with 57% and 70% for the ionic compounds (**3**) and (**5**), respectively. The latter were calculated from the respective crystal structures by considering both the cation and the anion[28] as spheres. We also note that the basal spacings of the intercalated phases (M^{II} = Cd or Mn[19]) belong to distinct ranges, 14.6–14.8 Å for [Fe(3,5-Cl_2-Sal_2Trien)]$^+$ and 19.1–19.3 Å for [Fe(5-OMe-Sal_2Trien)]$^+$, and the difference of the average values of *ca* 4.5 Å clearly exceeds the change in the molecular size expected for the ferric spin crossover. Consequently, these parameters are associated with differences of molecular shapes and/or arrangements within the interlayer region.

The molecular structures of the cations used for the preparation of the intercalates are considered in a first approach and the shapes of these cations are described by a parallelepiped. The interlayer spacing of ≈14.6 Å measured at room temperature for **9** (≈6.5 Å for $CdPS_3$) roughly compares with the smaller size of the molecular bulk (*ca* 9.8 Å with the van der Waals radii) of **1** and **3**. As a consequence, molecules are very likely to lie flattened along the interlayer direction and the contact area between molecules and the $CdPS_3$ layers has the largest value. The resulting host-guest ionic packings, which are expected to be maximised with this arrangement, may exert a significant chemical pressure on the cationic guests and thus lead to an additional stabilisation of their LS states. For [Fe(5-OMe-Sal_2Trien)]$^+$ intercalated in MPS_3 materials (19.3 Å for M = Cd and 19.1 Å for M = Mn), the very large interlayer parameters show that different arrangements and packings are adopted by the cations in the interlayer space. From the analysis of the crystallographic data of **5** and **7**, the previous values appear to be consistent with molecules lying this time with their larger size edge (≈19 Å with the van der Waals radii) nearly perpendicular to the MPS_3 sheets (see Fig. 8). The smaller host-guest packing forces should be balanced by some stabilising effects, probably those of hydrogen bonds with water molecules. The direct interactions between water molecules and cations that have been identified for **5** are also expected

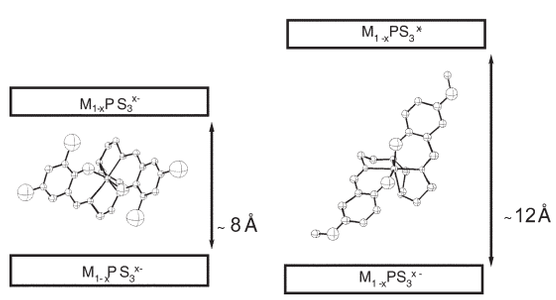

Fig. 8 Proposed arrangement of the cationic complexes **9** (left) and **10** (right) in the interlayer space.

for the MPS_3 intercalates. It has been shown in both cases that the water molecules are retained in these materials and that their removal contributes to the relative stabilisation of the HS species. Evidence for a cooperative spin transition associated with a thermal hysteresis has also been provided for the thoroughly dehydrated $MnPS_3$ intercalated material.[10] Such an experiment was out of the scope of the present study as the different $CdPS_3$ samples that were considered did not fulfil the criteria concerning the level of crystallinity and of structural ordering as shown by the X-ray diffraction patterns (reflection width), IR spectra [splitting of $\nu(PS_3)$ stretching modes] or the magnetic data (content of residual HS species). In addition, this comparison requires physical conditions[10] (cryogenic pumping at $p \sim 10^{-6}$ Torr, room temperature) that are not compatible with the measurements performed by a SQUID magnetometer.

Conclusion

In this investigation of some new ferric spin-crossover compounds, which derive from triethylene and substituted salicylaldehyde, we have shown that in the solid state different magnetic behaviours arising from HS, spin-crossover or LS species are achieved by varying either substituents or counter ions. The molecular structural characteristics determined from single crystal X-ray diffraction measurements were found to be consistent with the magnetic data at room temperature. It was also established that the magnetic properties of these compounds are dominated in the solid state by environmental factors due to packing, organisation and intermolecular interactions.

The intercalation of the two cationic species $[Fe(R\text{-}Sal_2\text{-}Trien)]^+$ into $CdPS_3$ leads to materials characterised by different arrangements of the complexes within the van der Waals gap. Magnetic measurements carried out on **9** and **10** provide evidence for effects due to the particular organisation in the $CdPS_3$ intercalates. **9** retains the LS state over a wide range of temperature whereas **10** exhibits a thermal spin equilibrium. In addition, these structural and magnetic characteristics of a cationic complex are similar in both MPS_3 intercalates (M = Cd and Mn). This shows that the molecular arrangement is due to the balance between guest-host and also guest-guest interactions. Thus, these 2D materials exhibiting the full set of spin-crossover behaviours are good candidates for the study of thermo- and photo-induced processes, all the more as they can be processed into thin layers. Investigation of such systems is currently in progress.

Acknowledgements

We thank Dr. A. Jaiswal and Dr. P. Delhaes from the Centre de Recherche Paul Pascal, Bordeaux, France, for EPR measurements. This work was financially supported by the European Union within a TMR network (EMR-FMRX-CT98-0199).

References

1 P. Gütlich, A. Hauser and H. Spiering, *Angew. Chem., Int. Ed. Engl.*, 1994, **33**, 2024; P. Gütlich, H. Spiering and A. Hauser, in *Inorganic Electronic Structure and Spectroscopy*, eds. E. I. Solomon and A. B. P. Lever, Wiley–VCH, Weinheim, 1999, vol. II, p. 575.
2 E. König, *Prog. Inorg. Chem.*, 1987, **35**, 527; E. König, *Structure and Bonding*, Springer–Verlag, Berlin, 1991, vol. 76, p. 51.
3 J. K. Beattie, *Adv. Inorg. Chem.*, 1988, **32**, 1.
4 M. Bacci, *Coord. Chem. Rev.*, 1988, **86**, 245.
5 H. Toftlund, *Coord. Chem. Rev.*, 1989, **94**, 67.
6 J. Zarembowitch, *New J. Chem.*, 1992, **16**, 255.
7 R. Clément and A. Léaustic, in *Magnetism: Molecules to Materials II, Molecule-Based Materials*, eds. J. S. Miller and M. Drillon, Wiley–VCH, Weinheim, 2001, p. 397; R. Clément, I. Lagadic, A. Léaustic, J.-P. Audière and L. Lomas, in *Chemical Physics of Intercalation II*, eds. P. Bernier, J. E. Fischer, S. Roth and S. A. Solin, Plenum Press, New York, 1993, p. 315; J. S. O. Evans, D. O'Hare, R. Clément, A. Léaustic, P. Thuery, *Adv. Mater.*, 1995, **7**, 735.
8 M. Nakano, S. Okuno, G.-E. Matsubayashi, W. Mori and M. Katada, *Mol. Cryst. Liq. Cryst.*, 1996, **286**, 83.
9 C. N. Field, M.-L. Boillot and R. Clément, *J. Mater. Chem.*, 1998, **8**, 283.
10 S. Floquet, S. Salunke, M.-L. Boillot, R. Clément, F. Varret, K. Boukheddaden and E. Rivière, *Chem. Mater.*, 2002, **14**, 4164.
11 A. Jaiswal, S. Floquet, M.-L. Boillot and P. Delhaes, *Chem. Phys. Chem.*, 2002, **12**, 5890.
12 R. Sieber, S. Decurtins, H. Stoeckli-Evans, C. Wilson, D. Yufit, J. A. K. Howard, S. C. Capelli and A. Hauser, *Chem.-Eur. J.*, 2000, **6**, 361.
13 M. F. Tweedle and L. J. Wilson, *J. Am. Chem. Soc.*, 1976, **98**, 4824.
14 K. L. Kadish, K. Das, D. Schaeper, C. L. Merrill and B. R. Welch, *Inorg. Chem.*, 1980, **19**, 2816; T. Zhu, C.-H. Su, D. Schaeper, B. K. Lemke and L. J. Wilson, *Inorg. Chem.*, 1984, **23**, 4345.
15 E. V. Dose, K. M. M. Murphy and L. J. Wilson, *Inorg. Chem.*, 1976, **15**, 2622; R. A. Binstead, J. K. Beattie, E. V. Dose, M. F. Tweedle and L. J. Wilson, *J. Am. Chem. Soc.*, 1978, **100**, 5609.
16 E. Sinn, G. Sim, E. V. Dose, M. F. Tweedle and L. J. Wilson, *J. Am. Chem. Soc.*, 1978, **100**, 3375.
17 Y. Nishida, K. Kino and S. Kida, *J. Chem. Soc., Dalton Trans.*, 1987, 1957.
18 Y. Maeda, H. Oshio, Y. Tanigawa, T. Oniki and Y. Takashima, *Hyperfine Interact.*, 1991, **68**, 157; Y. Maeda, H. Oshio, Y. Tanigawa, T. Oniki and Y. Takashima, *Bull.Chem. Soc. Jpn.*, 1991, **64**, 1522.
19 S. Floquet, Ph.D. Thesis, University of Paris-XI, Orsay, France, 2001.
20 G. M. Sheldrick, *SHELXS-97, Program for solution of crystal structures*, University of Göttingen, Germany, 1997; G. M. Sheldrick, *SHELXL-97, Program for refinement of crystal structures*, University of Göttingen, Germany, 1997.
21 P. G. Sim, E. Sinn, R. H. Petty, C. L. Merill and L. J. Wilson, *Inorg. Chem.*, 1981, **20**, 1213.
22 M. D. Timken, D. N. Hendrickson and E. Sinn, *Inorg. Chem.*, 1985, **24**, 3947; A. J. Conti, R. K. Chadha, K. M. Sena, A. L. Rheingold and D. N. Hendrickson, *Inorg. Chem.*, 1993, **32**, 2670.
23 H. Oshio, K. Toriumi, Y. Maeda and Y. Takashima, *Inorg. Chem.*, 1991, **30**, 4252; Y. Maeda, H. Oshio, K. Toriumi and Y. Takashima, *J. Chem. Soc., Dalton Trans*, 1991, 1227; Y. Maeda, Y. Noda, H. Oshio and Y. Takashima, *Bull. Chem. Soc. Jpn.*, 1992, **65**, 1825.
24 F. A. Deeney, C. J. Harding, G. G. Morgan, V. McKee, J. Nelson, S. T. Teat and W. Clegg, *J. Chem. Soc., Dalton Trans*, 1998, 1837; P. Guionneau, C. Brigouleix, Y. Barrans, A. E. Goeta, J.-F. Létard, J. A. K. Howard, J. Gaultier and D. Chasseau, *C. R. Acad. Sci., Ser. IIc: Chim.*, 2001, **4**, 161.
25 J. J. A. Kolnaar, Ph.D. Thesis, University of Leiden, Netherlands, 1998; Y. Garcia, Ph.D. Thesis, University of Bordeaux I, France, 1999.
26 M. S. Haddad, M. W. Lynch, W. D. Federer and D. N. Hendrickson, *Inorg. Chem.*, 1981, **20**, 123; M. S Haddad, W. D. Federer, M. W. Lynch and D. N. Hendrickson, *Inorg. Chem.*, 1981, **20**, 131.
27 E. König, *Chem. Rev.*, 1985, **85**, 219.
28 D. M. P. Mingos and A. L. Rohl, *Inorg. Chem.*, 1991, **30**, 3769.